Atmos. Chem. Phys. Discuss., 10, 1035–1082, 2010
www.atmos-chem-phys-discuss.net/10/1035/2010/

Atmospheric Chemistry and Physics Discussions

This discussion paper is/has been under review for the journal Atmospheric Chemistry and Physics (ACP). Please refer to the corresponding final paper in ACP if available.

Source apportionment of $PM_{2.5}$ in Cork Harbour, Ireland using a combination of single particle mass spectrometry and quantitative semi-continuous measurements

R. M. Healy, S. Hellebust, I. Kourtchev, A. Allanic, I. P. O'Connor, J. M. Bell, J. R. Sodeau, and J. C. Wenger

Department of Chemistry and Environmental Research Institute, University College Cork, Cork, Ireland

Received: 9 December 2009 – Accepted: 30 December 2009 – Published: 18 January 2010

Correspondence to: R. M. Healy (robert.healy@ucc.ie)

Published by Copernicus Publications on behalf of the European Geosciences Union.

Abstract

An aerosol time-of-flight mass spectrometer (ATOFMS) was co-located with a suite of semi-continuous instrumentation for the quantitative measurement of elemental carbon (EC), organic carbon (OC), sulfate, particle number and $PM_{2.5}$ mass at a site in Cork Harbour, Ireland for three weeks in August 2008. Off-line analysis of polar organic markers was also performed for the same period. The data collected was used to identify and apportion local and regional sources of $PM_{2.5}$. Over 550 000 ATOFMS particle mass spectra were generated and classified using the *K*-means algorithm. The vast majority of particles ionised by the ATOFMS were attributed to local sources, although one class of carbonaceous particles detected is attributed to North American or Canadian anthropogenic sources. The temporality of the ambient ATOFMS particle classes was subsequently used in conjunction with the semi-continuous measurements to apportion $PM_{2.5}$ mass using positive matrix factorisation. Six factors were obtained, corresponding to vehicular traffic, marine, long-range transport, power generation, domestic solid fuel combustion and shipping traffic. The estimated contribution of each factor to the measured $PM_{2.5}$ mass was 23%, 14%, 13%, 11%, 5% and 1.5%, respectively. Shipping was found to contribute 18% of the measured particle number (20–600 nm mobility diameter), and thus may have implications for human health considering the size and composition of ship exhaust particles.

1 Introduction

Ambient particulate matter is known to adversely affect human health, and long-term exposure to ultrafine (less than 100 nm diameter) ambient particles is expected to lead to irreversible changes in lung structure and function (Maier et al., 2008). Particulate matter also affects climate, both directly by scattering and absorbing solar radiation, and indirectly by providing sites for cloud condensation (IPCC, 2001). Identification of the various sources of anthropogenic particulate matter in urban environments has

ACPD

10, 1035–1082, 2010

received considerable attention with traffic, biomass burning and industrial processes typically contributing significantly to mass concentrations of particulate matter smaller than 2.5 µm in diameter ($PM_{2.5}$) (Castanho and Artaxo, 2001; Godoy et al., 2009; Karanasiou et al., 2009; Mugica et al., 2009; Heo et al., 2009). However, refined apportionment of $PM_{2.5}$ is often hindered by the low temporal resolution of off-line analysis and a lack of knowledge of the mixing state of the particles collected.

Single particle mass spectrometry allows the simultaneous detection of internally mixed primary and secondary ambient particle components including elemental and organic carbon, trace metals and ionic species with high temporal resolution (Sullivan and Prather, 2005). The internal mixing state of individual particles arising from particular anthropogenic and natural processes is often unique, and thus useful for identifying sources when combined with meteorological data (Reinard et al., 2007). Aerosol time-of-flight mass spectrometry (ATOFMS) has been employed in field studies to identify metal point sources such as steel manufacturing, smelting, refining and power generation facilities (Reinard et al., 2007; Snyder et al., 2009). More diffuse sources, such as light and heavy duty vehicular traffic and biomass burning, have also been identified using unique ATOFMS mass spectral signatures (Spencer et al., 2006; Silva et al., 1999; Moffet et al., 2007).

The positive matrix factorisation (PMF) (Hopke, 2003b) approach to source apportionment has recently been employed in the interpretation of data from aerosol mass spectrometers (Lanz et al., 2007; Allan et al., 2009; Dreyfus et al., 2009; Ulbrich et al., 2009) and has also been applied to a combination of data from an aerosol mass spectrometer and an aerosol time-of-flight mass spectrometer (Eatough et al., 2008). The latter study involved combining ATOFMS and time of flight aerosol mass spectrometry (ToF-AMS) data with continuous on-line and off-line quantitative measurements of $PM_{2.5}$, sulfate, nitrate, black carbon and several gas phase species in Riverside, California. PMF was performed with and without the mass spectral data, and the number of factors obtained rose from six to sixteen once the data was included. The additional factors introduced contributions from various local and regional sources includ-

ACPD
10, 1035–1082, 2010

ing shipping activity, thus demonstrating the value of on-line measurements of particle composition. More recently, sources of organic aerosol in Wilmington, Delaware, were apportioned using a photoionisation aerosol mass spectrometer (PIAMS) (Dreyfus et al., 2009). The single particle mass spectral data was modelled using PMF and these results were combined with elemental and organic carbon (EC/OC) quantitative data. Vehicular traffic was found to account for approximately two thirds of the organic carbon measured over an 18 day period.

The aim of this study was to identify and apportion local and regional sources of $PM_{2.5}$ in Cork Harbour using a combination of ATOFMS data and quantitative semi-continuous measurements of particle number, $PM_{2.5}$ mass, elemental carbon, organic carbon and sulfate and quantitative off-line measurements of polar organic marker compounds. ATOFMS mass spectral signatures for coal, peat and wood combustion particles were also obtained separately in order to apportion these sources more accurately in the ambient dataset. A PMF approach similar to that of Eatough et al. (2008) was employed for quantitative source apportionment based on the ATOFMS data collected.

2 Methodology

2.1 Sampling site and equipment

The sampling site and equipment are described in detail elsewhere (Healy et al., 2009). Briefly, the site is located at Tivoli Docks in the Port of Cork (51°54′5 N, 8°24′38 W), approximately 3 km east of Cork City centre. Shipping berths are located 400–600 m to the southwest and west-southwest. Residential areas surround the site on all sides except the north, northeast and east. The prevailing winds are south-westerly. A suite of semi-continuous instrumentation was located at the site for the duration of the campaign; SO_4^{2-} was monitored using a Thermo Electron model 5020 SPA instrument and EC/OC mass concentrations were measured using a thermal-optical carbon aerosol

ACPD
10, 1035–1082, 2010

analysis instrument (Sunset Laboratory Inc., field model 3rd generation) fitted with a cyclone to remove particles larger than 2.5 µm in diameter. A scanning mobility particle sizer (SMPS, TSI model 3081) collected particle number concentrations in the size range 20–600 nm (mobility diameter) every 3 min. A TEOM (tapered element oscillating microbalance, Thermo Electron model 1400a) was located on-site for the measurement of $PM_{2.5}$ mass concentrations (averaged every 30 min). The ATOFMS (TSI model 3800) was fitted with an aerodynamic lens (TSI model AFL100) for the measurement of particles in the size range 100–3000 nm. The instrument is described in detail elsewhere (Dall'Osto et al., 2004). In short, particles are sampled through an orifice and accelerated through the aerodynamic lens to the sizing region of the instrument. Here, the aerodynamic diameter of particles is calculated based on their time of flight between two continuous wave lasers (Nd:YAG, 532 nm). Particles are then transmitted to the mass spectrometry region of the instrument and ionised using a Nd:YAG laser (266 nm). The resulting positive and negative ions are finally analysed using two collinear time-of-flight mass spectrometers. Wind speed, wind direction, temperature, humidity and rainfall were monitored using a Casella NOMAD weather station. All instruments sampled air through stainless steel tubing from a height of 4 m above ground level. Every instrument was located on site for three weeks from 7–28 August 2008, except for the SMPS which was on site from 14–28 August 2008.

2.2 Off-line analysis of polar organic marker compounds

24 h $PM_{2.5}$ samples were collected on quartz fibre filters (Pallflex, 150 mm diameter, prebaked at 600 °C) using a high volume (Digitel) sampler with a flow rate of 500 L min^{-1}. The polar fraction of the $PM_{2.5}$ samples was extracted and analysed by GC/MS as described in detail elsewhere (Kourtchev et al., 2008, 2009a). Briefly, 6–12 cm^2 sections of each filter were used for extraction depending on the organic carbon loading. Each section was spiked with two internal recovery standards; 0.5 µg methyl-β-D-xylanopyranoside (MXP) and 0.5 µg deuterated (D_4)-succinic acid, and extraction was performed using a dichloromethane-methanol mixture (80:20, v/v). The extract

residues were trimethylsilylated with *N,O*-bis(trimethylsilyl)trifluoroacetamide containing 1% trimethylchlorosilane and immediately analysed by GC/MS. An aliquot of 1 µL was injected in the splitless mode. The GC/MS system consisted of an Agilent 6890N gas chromatograph (Agilent Technologies, Palo Alto, CA, USA) coupled to an Agilent 5795 quadrupole mass selective detector. The chromatographic column used was a cross-linked HP-5MS capillary column (5% phenyl, 95% methylpolysiloxane, 30 m×0.25 mm i.d., 0.25 mm film thickness, J&W Scientific, Palo Alto, CA, USA). The method parameters are outlined in detail in a previous article (Kourtchev et al., 2008).

2.3 Combustion experiment

Mass spectral signatures were obtained for coal, "smokeless" coal, peat and wood by burning each in turn for approximately 1 h in an outdoor stove and detecting the fresh combustion particles by ATOFMS. Each fuel was purchased locally in order to be representative of typical domestic output in the area. Specifically, commercially available compacted peat briquettes, bituminous coal, smokeless coal and ash wood were used. Peat is commonly used in Ireland for domestic space heating. Ash wood was used as it is widely available for sale in retail outlets and service stations in Cork City. 16 118 mass spectra were generated during the experiment and clustered using the *K*-means algorithm ($K=10$) as described in Sect. 2.4 (MacQueen, 1967). Coal, peat and wood burning particles were effectively clustered into separate classes although coal and smokeless coal did not exhibit sufficiently different mass spectra to be separated. These spectra were subsequently used to confirm the identification of classes in the ambient dataset.

2.4 ATOFMS data analysis

During the three week campaign 558,740 ATOFMS particle mass spectra were generated and subsequently imported into ENCHILADA (Environmental Chemistry through Intelligent Data Analysis), a freeware single particle data analysis software package

ACPD
10, 1035–1082, 2010

(Gross et al., 2006b; Snyder et al., 2009) and clustered using the K-means algorithm (MacQueen, 1967), (K=50). ENCHILADA has been previously used to classify ATOFMS mass spectra generated from ambient particles at sites in Switzerland and East St. Louis, Illinois (Herich et al., 2008; Snyder et al., 2009). Inhomogeneous clusters were clustered again using K-means when necessary in order to refine particle classification. Those clusters with similar mass spectra and temporality were recombined to generate the following 14 particle classes; coal, peat, wood, sea salt, shipping, Ca-traffic, EC-traffic, EC-phos-fresh, EC-phos-aged, EC-domestic, EC-background, EC-oil, OC, and oligomer. These classes account for 527 292 (94%) of the particle mass spectra generated. The EC-phos-fresh and EC-phos-aged classes were generated from one bimodal class. When separated the two modes exhibited completely different temporality and were thus separated by size. Particles of aerodynamic diameter less than 300 nm were classified as EC-phos-fresh and particles of aerodynamic diameter between 300 and 1000 nm were classified as EC-phos-aged. Hourly summed particle counts of each final particle class were subsequently used for positive matrix factorisation. Particle subclasses containing increased or additional signals for secondary species such as ammonium and nitrate were combined with their freshly emitted analogues for this analysis as they originate from the same source.

2.5 Positive matrix factorisation (PMF)

The fundamental relationship between an emission source and receptor (sampling location) can be expressed as follows (Hopke, 2003a):

$$X = \mathbf{G}\mathbf{F}^{\mathrm{T}} + E \quad (1)$$

where $\mathbf{G}$ is an $n \times p$ matrix representing source contributions to the samples, $\mathbf{F}^{\mathrm{T}}$ is the transpose of an $m \times p$ matrix of source profiles, $\mathbf{E}$ is the matrix of residuals, n is the number of samples, p is the number of variables and m is the number of extracted components or source categories. Each sample is an observation at a particular time, and thus $\mathbf{G}$ describes the temporal variation of the source contributions. The overall

ACPD
10, 1035–1082, 2010

dataset matrix is comprised of samples (rows) and variables (columns). A viable statistical solution to the expression is then sought, the aim of which is to minimise the residuals in **E**.

The PMF approach takes into account the uncertainties associated with each individual measurement, or data point (Paatero and Tapper, 1994; Hopke, 2003b; Ramadan et al., 2003). Hence the variables are weighted by a measure of trust in the individual measurements and adjusted to their detection limits. "Bad" samples can be down-weighted or excluded and the selected solution is based on goodness of fit. Results are also constrained to the non-negative, to avoid sources providing negative contributions to concentrations measured at the receptor sites. This approach reduces the likelihood of misinterpreting factor profiles.

The identification of factors can be improved by the inclusion of particle types that have been unequivocally assigned to a source through their unique mass spectra (Eatough et al., 2008). As with the study of Eatough et al. (2008), the factorisation procedure has been applied to the previously clustered single particle mass spectra obtained by ATOFMS in this work. The clustering procedure provides hourly counts of identified particle types that are treated as independent variables alongside hourly averages of measured EC, OC, SO_4 and $PM_{2.5}$ mass and SMPS particle number concentration. By combining this information it is possible to apportion PM mass in a quantitative manner. Furthermore, the benefit of using specific markers in factor identification is that it provides a better estimate for source contributions that may be too insignificant to influence hourly averages of common species in a predictable manner. This particularly applies to sources that are characterised by brief and/or irregular events or long-range emissions that bear no correlation to local events. The PMF model was developed using the USEPA PMF 3.0 software package available at www.epa.gov/scram001/receptorindex.htm. The uncertainty matrix associated with the data was calculated based on the instrumental level of detection and uncertainty (error fraction) as given by the manufacturer's documentation. The uncertainty used to describe the ATOFMS data was ±15% as in Eatough et al. (2008). For concentrations

ACPD
10, 1035–1082, 2010

less than or equal to the method detection limit (MDL) provided, the uncertainty was calculated using the relationship:

$$\text{Uncertainty} = \frac{5}{6} \times \text{MDL} \quad (2)$$

If the concentration was greater than the MDL provided, an alternative relationship was employed as follows:

$$\text{Uncertainty} = \sqrt{(\text{error fraction} \times \text{uncertainty})^2 + (\text{MDL})^2} \quad (3)$$

In performing PMF, the number of factors to be identified is defined by the user. However, a higher order solution does not necessarily contain the same factors as a lower order solution. Experimentation with the number of factors was performed until the most reasonable results were obtained. Estimation of the contribution of each factor to the total $PM_{2.5}$ mass was subsequently performed by scaling the PMF factor contributions (in the **G** matrix of Eq. 1) against measured $PM_{2.5}$ mass by regression (Maykut et al., 2003; Shi et al., 2009).

3 Results and discussion

3.1 Semi-continuous measurements and meteorology

The mean ambient mass concentrations of organic carbon (OC), elemental carbon (EC), sulfate and $PM_{2.5}$ measured at the site for the duration of the campaign were 1.13, 0.61, 0.49 and 9.67 $\mu g\, m^{-3}$, respectively, Table 1. These values are broadly in line with those observed at a different site in Cork City from July–August 2001 (Yin et al., 2005). Seasonal variation of these variables has been discussed in detail in a previous article (Hellebust et al., 2009b). Wind direction was predominantly south-westerly for the first and third weeks of the campaign and predominantly north-westerly from 14–23 August 2008. The average wind speed, air temperature and relative humidity were

4.7 m s^{-1}, 16 °C and 80%, respectively. Rainfall was observed between 9–12 August 2008, 15–18 August 2008 and on the 23 August 2008. The first seventeen days of the campaign were characterised by clean North Atlantic and subarctic air masses, while air masses originating in North America and Canada influenced the site from 24–28 August 2008.

3.2 ATOFMS particle classes

3.2.1 Coal, peat and wood

Coal, peat and wood particles accounted for 41%, 10% and 9% of the total particles successfully ionised and detected by the ATOFMS, and were observed almost exclusively in the submicron size range. Although particle counts have not been scaled for size-related transmission efficiency through the aerodynamic lens or composition-dependent ionisation efficiency, the results indicate that, even during the summer months, domestic solid fuel combustion is a source of $PM_{2.5}$ in Cork Harbour. The emission factors of carbonaceous particulate matter for the combustion of coal in domestic stoves have been demonstrated to be up to 100 times higher than those from industrial boilers (Zhang et al., 2008). A recent source apportionment study performed in Krakow, Poland, estimated that domestic coal burning accounted for over 50% of the measured PM_{10} mass during a typical winter pollution episode (Junninen et al., 2009). The clustering procedure used in this work allowed for the separation of freshly emitted and aged combustion particles into subclasses. These subclasses were recombined for positive matrix factorisation as they originate from the same source. Fresh ambient combustion particles were identified based on their similarity to particles generated from each fuel during the combustion experiment. Figures 1–3 compare average dual ion mass spectra for freshly emitted ambient "coal-fresh", "peat-fresh" and "wood-fresh" clusters with those generated during the experiment. Coal-fresh positive ion mass spectra are characterised by carbon and hydrocarbon ions (*m/z* 12, $[C]^+$; 27, $[C_2H_3]^+$; 36, $[C_3]^+$; 37, $[C_3H]^+$; 48, $[C_4]^+$; 50, $[C_4H_2]^+$; 60, $[C_5]^+$) and a relatively low signal for

sodium (*m/z* 23, $[Na]^+$) and potassium (*m/z* 39, 41, $[K]^+$). Negative ion mass spectra contain peaks corresponding to carbon (*m/z* −24, $[C_2]^-$; −36, $[C_3]^-$; −48, $[C_4]^-$; −60, $[C_5]^-$), carbon-nitrogen adducts (*m/z* −26, $[CN]^-$; −42, $[CNO]^-$), nitrate (*m/z* −46, $[NO_2]^-$; −62, $[NO_3]^-$), and sulfate (*m/z* −80, $[SO_3]^-$; −81, $[HSO_3]^-$; −97, $[HSO_4]^-$. Although none of these ions are individually unique to the combustion of coal, there is a very strong similarity in the relative ion intensities of freshly emitted coal combustion particles and the ambient coal-fresh particles as shown in Fig. 1. Particles measured by ATOFMS in an aerosol outflow from Asia that were tentatively assigned to coal burning exhibited different spectra to those observed in this work, sharing many of the same positive ions but with an additional signal for lithium (Guazzotti et al., 2003). No signal was observed for lithium in coal combustion particles either during the combustion experiment or in the ambient dataset in this work (Fig. 1), although trace metal impurities are likely to depend on the origin of the coal. Single particle mass spectra generated with a single particle analysis and sizing system (SPASS) containing a signal for carbon but not for sulfate, were attributed to a fresh domestic coal combustion source in a recent study performed in Krakow, Poland (Mira-Salama et al., 2008). In that case no combustion spectra were generated to confirm the source. In this work, however, a strong signal for sulfate was consistently observed even in freshly emitted coal combustion particles (Fig. 1).

Peat-fresh particles are characterised by much higher signals for sodium (*m/z* 23, $[Na]^+$) and potassium (*m/z* 39, 41, $[K]^+$) which dominate the positive ion mass spectra, although similar carbon and hydrocarbon fragments to those observed for coal are also present (Fig. 2). Negative ion mass spectra for coal-fresh and peat-fresh particles contain many of the same ions but at very different relative intensities, with peat-fresh particle spectra exhibiting additional signals for chloride (*m/z* −35, −37, $[Cl]^-$) and much lower signals for sulfate (*m/z* −97, $[HSO_4]^-$).

Wood-fresh positive ion mass spectra are dominated by potassium cations (*m/z* 39, 41, $[K]^+$) while positive carbon and hydrocarbon ions are almost completely suppressed. A signal for sodium (*m/z* 23, $[Na]^+$) is also present but at a significantly lower

relative intensity than in peat-fresh particles. Potassium chloride adducts, possibly formed during the desorption-ionisation process, are often also observed (*m/z* 113, 115, $[K_2Cl]^+$). Negative ion mass spectra for wood-fresh particles are very different to those observed for peat-fresh and coal-fresh particles, containing both elemental carbon ions (*m/z* −24, $[C_2]^-$; −36, $[C_3]^-$; −48, $[C_4]^-$) and oxidised organic carbon fragments (*m/z* −45, $[HCOO]^-$; −59, $[CH_3COO]^-$; *m/z* −89, $[COOHCOO]^-$) (Silva et al., 1999; Silva and Prather, 2000). The latter fragment corresponds to oxalate, a species often observed in biomass burning particles (Kundu et al., 2009; Yang et al., 2009). Signals are also observed for chloride (*m/z* −35, −37, $[Cl]^-$), carbon-nitrogen adducts (*m/z* −26, $[CN]^-$; −42, $[CNO]^-$), nitrate (*m/z* −46, $[NO_2]^-$; −62, $[NO_3]^-$), and sulfate (*m/z* −80, $[SO_3]^-$; −81, $[HSO_3]^-$; −97, $[HSO_4]^-$ (Fig. 3). Similar ATOFMS mass spectra have been observed for particles arising from the combustion of various plant species indigenous to California (Silva et al., 1999). ATOFMS particle mass spectra with intense signals for potassium have also been previously assigned to biomass burning during the Indian Ocean Experiment, in Mexico City and in Sweden (Guazzotti et al., 2003; Moffet et al., 2007; Friedman et al., 2009). Spectra generated from wood burning particles during the combustion experiment exhibit almost identical positive ion mass spectra to those observed in the ambient dataset, and also share many of the same ions in the negative ion mass spectra. However the particles generated during the combustion experiment contain much higher signals at *m/z* −43 and −59, probably corresponding to the oxidised organic carbon fragments $C_2H_3O^-$ and CH_3COO^-, respectively. The latter is also present in ATOFMS mass spectra generated from nebulised levoglucosan (Silva et al., 1999; Silva and Prather, 2000; Guazzotti et al., 2003). It is possible that this difference is due to the presence of semi-volatile oxidised organics in the combustion experiment particles that may undergo evaporation in transit, thus reducing their signal in the ambient wood-fresh particles. However, another possible explanation is that a combination of different species of wood are burned in the local area which give rise to different mass spectra.

Aged coal particle subclasses were also observed; one exhibiting an additional sig-

nal for ammonium (*m/z* 17, $[NH_3]^+$; 18, $[NH_4]^+$), "coal-amm", and another containing a signal for ammonium and an increased signal for nitrate (*m/z* −46, $[NO_2]^-$; −62, $[NO_3]^-$), "coal-amm-nit". Similarly, aged peat, "peat-nit", and wood, "wood-nit", particle subclasses were also observed which exhibited higher signals for nitrate but no additional signal for ammonium. Cork City is surrounded by agricultural land and gas phase ammonia is expected to be ubiquitous. The absence of ammonium ions in aged peat and wood mass spectra could be due to the presence of increased levels of potassium and sodium causing a suppression of ammonium positive ion signals coupled with the relatively low sensitivity of ATOFMS for ammonium (Spencer et al., 2006; Gross et al., 2000). However it is also possible that coal combustion particles, which contain much more sulfate than those produced by peat or wood combustion (Figs. 1–3), undergo heterogeneous reaction with gas phase ammonia more readily. This is supported by the fact that there is little or no delay between the appearance of the coal-fresh and coal-amm classes, indicating rapid uptake of ammonium. The average dependence of the various coal, peat and wood subclasses on time of day is shown in Fig. 4. The average diurnal profile for the three freshly emitted particle types is very similar, increasing sharply from 18:00 to 21:00 h, and decreasing sharply after 22:00 h. The periods of increasing and decreasing particle number can be explained by the local population lighting fires and allowing them to extinguish, respectively. The subclasses coal-amm-nit, peat-nit and wood-nit exhibit a dependence on later night-time and early morning hours, albeit less pronounced in the case of wood-nit, indicating that they are aged and have had time to form additional nitrate. Biomass burning particles detected by ATOFMS in Mexico City have previously been separated into fresh and aged subclasses based on nitrate ion intensity (Moffet et al., 2007). The highest numbers of nitrated coal, peat and wood particles were observed during four distinct events beginning on the evenings of the 11, 13, 14 and 22 August 2008. Each event coincided with a drop in wind speed to levels below 1 m s^{-1} as shown in Fig. 5. These periods of low wind speed allow locally emitted combustion particles to undergo prolonged mixing with gas phase NO_2. Under these conditions NO_2 can be oxidised to yield nitric acid

ACPD
10, 1035–1082, 2010

at particle surfaces. In the presence of particle phase water, N_2O_5 and NO_3 can also be hydrolysed to form nitric acid (Mogili et al., 2006; Wang et al., 2009). Gas phase nitric acid or pre-existing ammonium nitrate can also be directly taken up (Sullivan et al., 2007). Heterogeneous reaction of gas phase nitric acid with sodium chloride on sea salt particle surfaces can result in the formation of particle phase sodium nitrate and gas phase hydrochloric acid as demonstrated previously using ATOFMS (Gard et al., 1998). While it may be possible that some sodium and potassium cations on coal, peat and wood combustion particle surfaces are available for heterogeneous reaction with gas phase nitric acid, simple uptake through adsorption, condensation or N_2O_5/NO_3 hydrolysis are expected to be the dominant processes. A strong correlation between nitrate-containing particles detected using ATOFMS and relative humidity was observed during a recent pollution episode in Shanghai (Wang et al., 2009). Coincident increases in nitrate-containing particle counts and O_3 and NO_2 mixing ratios suggested that N_2O_5 and NO_3 hydrolysis at particle surfaces dominated particulate nitrate formation at night during these episodes.

Interestingly, the appearance of the nitrated subclasses occurs in the following temporal order: wood-nit, peat-nit, coal-amm-nit (Fig. 4). This phenomenon could be related to varying hygroscopic properties within these particle classes. Amazonian, North American and Swedish biomass burning particles have been measured with hygroscopic growth factors of up to 1.26 at 90% relative humidity, 1.29 at 80% relative humidity and 1.40 at 82% relative humidity, respectively (Rissler et al., 2006; Carrico et al., 2005; Herich et al., 2009). On average, relative humidity at the site ranged from 74–89% between 20:00 h and 10:00 h for the measurement period, and the vast majority of nitrated particles were observed between these times. If coal-fresh particles contain less oxidised water-soluble organic material than wood-fresh particles, as suggested by their respective mass spectra (Figs. 1 and 3), they should exhibit lower hygroscopic growth factors. A delay in the uptake of water, necessary for N_2O_5 and NO_3 hydrolysis, would explain the delay in the appearance of coal-amm-nit particles relative to wood-nit particles. The appearance of peat-nit particles occurs between

coal-amm-nit and wood-nit (Fig. 4), suggesting an intermediate hygroscopic growth factor, which is expected considering that peat is composed of decayed vegetation and is a coal precursor. Nitrated subclasses were observed at night when nitrate radical concentrations, and therefore N_2O_5 concentrations, should be at their highest. Thus it appears that N_2O_5 and NO_3 hydrolysis are also an important source of particle phase nitrate in Cork Harbour. While very strongly dependent upon time of day, none of the domestic combustion classes exhibited an obvious dependence on wind direction due to the abundance of residential areas surrounding the site.

All three domestic combustion particle classes are very well correlated with each other (R^2>0.90, least squares linear regression), indicative of a single source, Table 2. Particle counts for these classes, when summed over 24 h intervals, are also well correlated with 24 h resolution off-line quantitative GC/MS measurements of levoglucosan, mannosan and galactosan. These species arise from the thermal degradation of cellulose and are well-established markers for biomass burning (Pashynska et al., 2002; Simoneit et al., 2004; Kourtchev et al., 2008). The ambient mass concentrations of these compounds are not the focus of this study and will be reported in a future publication. One visually obvious outlier was removed, the data point for the 22 August 2008, increasing the R^2 value for the linear regression of wood particle counts and levoglucosan mass from 0.57 to 0.81. Correlation coefficients for the ATOFMS classes and biomass burning markers are given in Table 2. All three classes are very well correlated with levoglucosan (R^2=0.81–0.82), although the correlation between the ATOFMS classes and the other polar organic markers, galactosan and mannosan, is lower. In fact, the correlation between these two compounds and levoglucosan is also much lower than expected considering that all three arise from the same source. This is because galactosan and mannosan are present at much lower mass concentrations than levoglucosan in the extracts and are often close to the detection limit of the GC/MS. Similar off-line analysis was performed for filters collected during a subsequent campaign at the same site in February 2009. In that case there was a much larger contribution from biomass burning and thus much higher GC/MS responses

ACPD
10, 1035–1082, 2010

for the corresponding marker compounds, resulting in improved correlation between galactosan, mannosan and levoglucosan (R^2=0.97–0.99) (Kourtchev et al., 2009b).

3.2.2 Sea salt

Sea salt particles accounted for 12% of those ionised and did not exhibit a strong dependence on time of day, although a slight dependence on westerly and south-westerly wind direction was observed. These particles were characterised by sodium (*m/z* 23, $[Na]^+$; *m/z* 46, $[Na_2]^+$), magnesium (*m/z* 24, $[Mg]^+$) and calcium (*m/z* 40, $[Ca]^+$) ions, sodium oxide/hydroxide adducts (*m/z* 62, $[Na_2O]^+$; *m/z* 63, $[Na_2OH]^+$) and sodium chloride adducts (*m/z* 81, 83, $[Na_2Cl]^+$) in the positive ion mass spectra. Negative ion mass spectra contained signals for sodium (*m/z* −23, $[Na]^-$), chloride (*m/z* −35, −37, $[Cl]^-$), nitrate (*m/z* −46, $[NO_2]^-$; −62, $[NO_3]^-$), sodium chloride adducts (*m/z* −58, −60, $[NaCl]^-$; −93, −95, −97, $[NaCl_2]^-$) and sulfate (*m/z* −80, $[SO_3]^-$). An average mass spectrum of the sea salt class is given in Fig. 6. A subclass with higher signals for nitrate, presumably formed through heterogeneous reaction with nitric acid, was also observed but did not exhibit a strong dependence on time of day. Pure and nitrated sea salt classes have been previously observed during ATOFMS field campaigns (Gard et al., 1998; Dall'Osto et al., 2004).

3.2.3 Shipping

Shipping particles exhibited a very strong dependence on west-south-westerly wind direction but little or no dependence on time of day and accounted for approximately 4% of the particles ionised. These particles were observed in short, sharp events and attributed to ships entering and departing from the nearby shipping berths. This was confirmed through comparison with the Port of Cork shipping logs as outlined in a previous article (Healy et al., 2009). The positive ion mass spectra are characterised by organic and elemental carbon (*m/z* 12, $[C]^+$; 27, $[C_2H_3]^+$; 36, $[C_3]^+$; 37; $[C_3H]^+$), sodium (*m/z* 23, $[Na]^+$), calcium (*m/z* 40, $[Ca]^+$), iron (*m/z* 56, $[Fe]^+$), vanadium (*m/z*

51, $[V]^+$; 67, $[VO]^+$) and nickel (*m/z* 58, $[Ni]^+$) ions. Negative ion mass spectra contain signals for elemental carbon (*m/z* −12, $[C]^-$; −24, $[C_2]^-$; −36, $[C_3]^-$; −48, $[C_4]^-$), carbon-nitrogen adducts (*m/z* −42, $[CN]^-$) and sulfate (*m/z* −64, $[SO_2]^-$; −80, $[SO_3]^-$; 81, $[HSO_3]^-$; −97, $[HSO_4]^-$) ions (Fig. 6).

3.2.4 Ca-traffic, EC-traffic, EC-phos-fresh and EC-phos-aged

Three particle classes were observed that exhibited an obvious dependence on daytime vehicular traffic hours as shown in Fig. 7; Ca-traffic, EC-traffic and EC-phos-fresh. These classes peak on average between 08:00 and 17:00 h and decrease dramatically between 00:00 and 06:00 h, as expected for vehicular activity. An additional increase is observed between 20:00 and 22:00 h for EC-traffic although this may be partly due to incorrect classification of some domestic solid fuel combustion particles (EC-domestic), which exhibit almost identical negative ion mass spectra (Figs. 6 and 8). The Ca-traffic, EC-traffic and EC-phos-fresh particle classes combined account for approximately 9% of the particles successfully ionised.

Ca-traffic particles have a relatively wide size distribution, with aerodynamic diameters ranging from 150–3000 nm, possibly even wider as these are the lower and upper size limits of the TSI 3800 ATOFMS particle detection range due to limited light scattering and aerodynamic lens (TSI model AFL100) transmission efficiency, respectively. At first the larger particles were assumed to be resuspended crustal material due to their size, the predominance of calcium ions, and the absence of carbon ions in the positive ion mass spectra (Fig. 6). On closer inspection these spectra were found to exhibit a very strong similarity to those generated from atomised engine oil, which contains calcium as an additive, thus suggesting that these are most likely vehicle exhaust particles containing a significant amount of unburned oil (Spencer et al., 2006). Ca-traffic positive ion spectra are characterised by signals for calcium (*m/z* 40, $[Ca]^+$) and calcium oxide/hydroxide adducts (*m/z* 56, $[CaO]^+$; 57, $[CaOH]^+$; 96, $[Ca_2O]^+$), and negative ion mass spectra contain signals for nitrate (*m/z* −46, $[NO_2]^-$; −62, $[NO_3]^-$), phosphate (*m/z* −63, $[PO_2]^-$; −79, $[PO_3]^-$; −95, $[PO_4]^-$) and sulfate (*m/z* -81, $[HSO_3]^-$;

−97, $[HSO_4]^-$).

EC-traffic particles are smaller in size, with aerodynamic diameters in the range 100–600 nm and exhibit positive ion mass spectra containing typical elemental carbon fragments (*m/z* 12, $[C]^+$; 24, $[C_2]^+$; 84, $[C_7]^+$) along with signals for sodium (*m/z* 23, $[Na]^+$) and calcium (*m/z* 40, $[Ca]^+$). Negative ion spectra contain signals for elemental carbon (*m/z* −12, $[C]^-$; −24, $[C_2]^-$; −84, $[C_7]^-$) and a relatively low response for sulfate (*m/z* −97, $[HSO_4]^-$) (Fig. 6). Similar particles have been observed previously by ATOFMS in freshly emitted vehicle exhaust both in a laboratory dynamometer study and at a roadside site (Toner et al., 2006, 2008).

EC-phos-fresh particles exhibit similar positive ion mass spectra to those in the EC-traffic class, although much lower signals for sodium and calcium are observed (Fig. 8). The negative ion mass spectra are also quite similar but contain an additional signal for phosphate (*m/z* −79, $[PO_3]^-$) arising from phosphorous-containing additives in motor oil. This particle class has also been observed in previous ATOFMS vehicle exhaust studies (Toner et al., 2006, 2008) and can be attributed to local traffic due to its strong diurnal trend (Fig. 7).

EC-phos-aged particles, accounting for approximately 1.5% of the particles ionised, have very similar positive ion mass spectra to EC-phos-fresh particles but do not contain any signal for $[PO_3]^-$ in the negative ion mode (Fig. 8). However, a strong signal is observed instead at *m/z* −95, possibly due to $[PO_4]^-$, suggesting that EC-phos-aged particles may represent an oxidised or aged form of EC-phos-fresh particles. When compared to EC-phos-fresh mass spectra, a much higher signal is observed for sulfate (*m/z* −97, $[HSO_4]^-$) relative to the negative elemental carbon ions and an additional signal corresponding to oxalate (*m/z* −89, $[COOHCOO]^-$) is also present. Assuming that both EC-phos-fresh and EC-phos-aged particles are generated in the same way, the differences in the negative ion mass spectra suggest that uptake of sulfate and oxalic acid has occurred during transport in the case of the latter, a process previously observed for transported mineral dust particles in Asia (Sullivan and Prather, 2007). Oxalic acid has also been detected in single particles arising from biomass and fossil

fuel combustion processes in Mexico City and Shanghai, and may be directly emitted at source or formed through the oxidation of biogenic and anthropogenic volatile organic compounds (VOCs) in the gas or aqueous phases (Moffet et al., 2007; Carlton et al., 2007; Hallquist et al., 2009; Yang et al., 2009). Accumulation of secondary species would account for the much larger aerodynamic diameter of these particles (300–1000 nm) compared to EC-phos-fresh (100–300 nm). EC-phos-aged particles do not appear in any significant number until the last 4 days of the campaign (24–28 August 2008), during which elevated counts are consistently observed as shown in Fig. 9. These particles do not exhibit any dependence on time of day but are strongly dependent on west-southwesterly wind direction. 5 day air mass back-trajectories, calculated using the Hybrid Single-Particle Lagrangian Integrated Trajectory (HYSPLIT) dispersion model (Draxler and Rolph, 2003), demonstrate that air masses arriving at 500, 1000 and 2000 m above the site during this 4 day period originated in North America and Eastern Canada (Fig. 10, right panel), while for the rest of the campaign (7–23 August 2008) similar 5 day back-trajectories show that air masses consistently originated in the North Atlantic and Arctic Oceans (Fig. 10, left and middle panels). Back-trajectories for air masses arriving at 100 and 200 m above ground level were also calculated yielding similar results. Transatlantic transport to Europe of boreal forest fire particles originating in Canada and anthropogenic trace gases including O_3, CO, NO_y and VOCs originating in North America has been previously reported (Forster et al., 2001; Stohl et al., 2003). Another possible assignment for the fragment at *m/z* −95 ion is methanesulfonate $[CH_3SO_3]^-$ (Silva and Prather, 2000). Methylsulfonic acid aerosol can be formed through the oxidation of biogenic dimethylsulfide emitted from ocean surfaces (Andreae and Crutzen, 1997; Hallquist et al., 2009), and may have been accumulated by EC-phos-aged particles during transatlantic transport. This class may thus represent vehicle exhaust particles originally emitted in North America or Canada that have undergone oxidation and accumulation processes in transit before arriving at the Cork Harbour site.

3.2.5 EC-domestic, EC-background, EC-oil, OC and oligomer

The EC-domestic class accounts for approximately 1% of the particles ionised, and is characterised by positive ion mass spectra containing high signals for sodium (*m/z* 23, $[Na]^+$) and potassium (*m/z* 39, 41 $[K]^+$), Fig. 8. Negative ion mass spectra are almost identical to those observed for EC-traffic. As shown in Fig. 7, this class exhibits a similar diurnal variation to those observed for the coal, peat and wood classes. This temporality coupled with the presence of sodium and potassium ions in the positive ion mass spectra, also observed for coal and peat particles (Figs. 1 and 2), indicate that domestic combustion is the most likely source of these particles. A nitrated subclass is not observed for this particle class and is most likely explained by the poor hygroscopic growth factor of elemental carbon particles (Weingartner et al., 1997).

EC-background particles account for 4% of the particles ionised and are characterised by higher order elemental carbon fragments than any of the other classes ($[C]^+$, $[C_2]^+$, $[C_{11}]^+$, $[C]^-$, $[C_2]^-$, $[C_{11}]^-$). Signals are also observed for sodium (*m/z* 23, $[Na]^+$) and potassium (*m/z* 39, $[K]^+$) (Fig. 8). These particles do not exhibit any dependence on wind direction or time of day, suggesting multiple sources. Particles exhibiting very similar mass spectra and temporality have been previously observed using ATOFMS in Athens, Greece, and were attributed to fossil fuel combustion (Dall'Osto and Harrison, 2006).

EC-oil particles also do not exhibit a strong dependence on time of day or wind direction and account for 0.7% of the particles ionised. These particles exhibit positive ion mass spectra with signals for carbon (*m/z* 12, $[C]^+$; 24, $[C_2]^+$; 27, $[C_2H_3]^+$; 36, $[C_3]^+$), sodium (*m/z* 23, $[Na]^+$), potassium (*m/z* 39, 41 $[K]^+$) and calcium (*m/z* 40, $[Ca]^+$; 56, $[CaO]^+$) (Fig. 11). Negative ion mass spectra are dominated by a large signal for phosphate (*m/z* −63, $[PO_2]^-$; −79, $[PO_3]^-$). Similar particles have been observed in heavy duty vehicle exhaust using ATOFMS but without a signal for potassium, indicating that this class may contain some incorrectly classified particles and thus have more than one source (Toner et al., 2006).

ACPD
10, 1035–1082, 2010

The OC class accounts for approximately 3% of the particles ionised. OC particles are characterised by signals for carbon (*m/z* 12, $[C]^+$; 24, $[C_2]^+$; 36, $[C_3]^+$) and potassium (*m/z* 39, $[K]^+$) (Fig. 11). Although less obvious in Fig. 6 due to their relatively low signals, peaks are also consistently observed for ammonium (*m/z* 17, $[NH_3]^+$; 18, $[NH_4]^+$) and oxidised organic carbon (*m/z* 43, $[C_2H_3O]^+$). The negative ion mass spectra are characterised by an intense signal for sulfate (*m/z* −96, $[SO_4]^-$). This class was previously tentatively identified as transported ship exhaust particles due to their similarity to particles detected in San Diego using ATOFMS (Healy et al., 2009; Ault et al., 2009). However, the absence of any useful marker ions coupled with a lack of dependence on time of day or wind direction suggests multiple sources may emit these particles locally. Positive matrix factorisation helps to resolve the sources of this class, as outlined below. A similar class was also observed in Athens during a previous ATOFMS study (Dall'Osto and Harrison, 2006).

The oligomer class accounts for approximately 2% of the particles ionised. As shown in Fig. 7, these particles exhibit a very similar diurnal variation to the coal, peat and wood fresh and aged combustion classes. As for the aged domestic combustion classes, the highest numbers for this class are observed during low wind speed conditions. Oligomer particle mass spectra exhibit little or no signal for positive ions. When positive ion signals are present they correspond to carbon (*m/z* 12, $[C]^+$; 27, $[C_2H_3]^+$; 36, $[C_3]^+$), oxidised carbon (*m/z* 43, $[C_2H_3O]^+$), sodium (*m/z* 23, $[Na]^+$) and potassium (*m/z* 39, $[K]^+$), ions also associated with domestic combustion. Negative ions are consistently observed for oxidised organic carbon (*m/z* −45, $[HCOO]^-$; −59, $[CH_3COO]^-$; −89, $[COOHCOO]^-$), carbon-nitrogen adducts (*m/z* −26, $[CN]^-$), chloride (*m/z* −35, −37, $[Cl]^-$), nitrate (*m/z* −46, $[NO_2]^-$; −62, $[NO_3]^-$), and sulfate (*m/z* −80, $[SO_3]^-$; −81, $[HSO_3]^-$; −97, $[HSO_4]^-$ (Fig. 11). Higher mass negative ion signals are also observed up as far as *m/z* −400, but at much lower relative intensities (Fig. 11). ATOFMS particle mass spectra containing similar high mass negative ion signals have been identified as oligomer-containing, both in simulation chamber experiments and in ambient datasets (Gross et al., 2006a; Denkenberger et al., 2007). In the latter study, several different

aged particle types were found to contain oligomers, including vanadium-rich, amine-rich, organic carbon, and internally mixed organic/elemental carbon particles. Biomass burning particles did not contain any oligomeric species in that case. The oligomer-containing particles detected in this work exhibit a peak in particle number around 21:00 or 22:00 h, coinciding with the domestic solid fuel combustion classes (Fig. 7). This indicates that a significant fraction of these oligomer-containing particles are relatively fresh. Ions that are typically used to identify significantly aged ambient particles by ATOFMS include *m/z* −125 and *m/z* −195, corresponding to $[H(NO_3)_2]^-$ and $[H_2SO_4HSO_4]^-$, respectively (Moffet et al., 2007; Denkenberger et al., 2007). These ions are absent for the oligomer class identified in this work, again suggesting that these particles are relatively fresh compared to those observed by Denkenberger et al. (2007). The rate of formation of detectable oligomers in secondary organic aerosol is typically of the order of hours (Kalberer et al., 2004; Gross et al., 2006a). However their coincident appearance with fresh domestic combustion particles at early evening hours in this work suggests relatively rapid formation (Fig. 7).

3.3 Source apportionment

The PMF analysis was performed using the ATOFMS particle classes and quantitative EC/OC, sulfate, particle number and $PM_{2.5}$ data. Uncertainties were estimated as described above, but some data points were given higher uncertainty values based on assessment of their temporal trends in the context of all variables. The uncertainties for the following data points were increased significantly, to a value of 100; EC-oil on 21 August 2008 at 22:00 and 23:00 and EC-domestic on 21 August 2008 at 08:00. Six-, seven- and eight-factor solutions were explored. The source categories identified by the six-factor solution are described as: traffic, marine, long-range transport, power generation, domestic solid fuel combustion, and shipping. All factor profiles are identical in the six- and seven-factor solutions, except that the traffic factor is split into two for the latter. The ATOFMS particle classes EC-oil, Ca-traffic and EC mass are distributed into one of the new factors, and the EC-traffic and EC-phos-fresh classes

are distributed into the other. When the mass contribution of each factor is estimated, the two traffic factors obtained by the seven-factor solution combine to a total of 24% of total $PM_{2.5}$ mass. In the six-factor solution, the traffic source contributes an estimated 23%. The total $PM_{2.5}$ mass accounted for in the six-factor and the seven-factor solutions were 66.4% and 64.6%, respectively. An eight-factor solution results in splitting of the factors identified as traffic and domestic solid fuel combustion in the six-factor solution, and the mass apportioned increases marginally to 67.9% of the total. The six-factor solution appears to be the most appropriate to describe the data as no useful information is gained by increasing the number of factors. The estimated contributions of each factor to the measured $PM_{2.5}$ mass and each variable are given in Table 3.

3.3.1 Traffic

The traffic factor contributes the most to the ambient $PM_{2.5}$ mass (23%) and contributes significantly to particle number (42%), EC mass (43%), and the Ca-traffic and EC-phosfresh ATOFMS particle classes (83% and 82%, respectively). The high contributions to the ATOFMS classes indicate that their classification as traffic exhaust particles is correct. The contribution to EC-traffic is lower at 59%, and can be explained by the similarity of EC-traffic and EC-domestic negative ion mass spectra (Figs. 6 and 8). The domestic solid fuel combustion factor contributes 25% to the EC-traffic class, suggesting that an incorrect classification of some of these particles has occurred during the clustering of the ATOFMS mass spectra.

3.3.2 Marine

The marine factor contributes the most to the ATOFMS sea salt class as expected (86%), and contributes 14% to the $PM_{2.5}$ mass. Interestingly, this factor also has the second highest contribution to OC mass (20%), indicating that biological activity in the Atlantic Ocean is contributing to particulate matter in Cork Harbour. There is no additional ATOFMS class that is covariant with sea salt, suggesting that the instrument

ACPD
10, 1035–1082, 2010

is unable to detect these particles. This could be due to the absence of any chemical species that can absorb the wavelength of the UV laser (266 nm). This factor was not observed in a previous study using PMF on real-time data from the same site, but without ATOFMS particle speciation (Hellebust et al., 2009b). That study was performed over a longer period (May–August 2008), and only three factors corresponding to traffic, domestic combustion and power generation were identified and estimated to contribute 19%, 14% and 31% to the measured $PM_{2.5}$ mass. The contribution of domestic solid fuel combustion and power generation to the measured $PM_{2.5}$ mass in this work are lower, as expected considering the introduction of three new factors (Table 3). The introduction of additional factors is analogous to the work of Eatough et al. (2008), who also observed additional factors when ATOFMS and AMS datasets were added to existing real-time monitoring data.

3.3.3 Long-range transport

The long-range transport factor was not resolved in the previous Cork Harbour study, due to the absence of ATOFMS mass spectral data. A very high loading for the ECphos-aged class was observed for this factor indicating that it represents regionally transported aerosol from North America or Canada. Contributions of 18%, 11% and 15% to OC mass, EC mass and sulfate mass, respectively, indicate that transatlantic particles can impact upon air quality in Ireland. Although this regional episode only persisted for 4 days out of the total measurement period of 21 days it is estimated to contribute 13% to the $PM_{2.5}$ mass measured over the entire campaign. This factor also accounts for 10% and 31% of the contribution to the sea salt and OC ATOFMS classes.

3.3.4 Power generation

The power generation factor represents a source which would not have been identified by ATOFMS particle classification without PMF analysis, and exhibits variable contributions of 16%, 18% and 40% to OC mass, EC mass and sulfate mass, respectively. This

factor is estimated to contribute 11% to the measured $PM_{2.5}$ mass. A coal-fired power generation facility lies to the southeast of the sampling site, directly across the harbour and explains the relatively high contribution to the ATOFMS coal class (30%) (Hellebust et al., 2009b). A high contribution to the OC particle class is also observed (69%), which indicates that this class is accounted for almost exclusively by the long-range transport and power generation factors. A contribution of 35% to the EC-background class is observed, although this class is distributed among several other factors suggesting input from every combustion source.

3.3.5 Domestic solid fuel combustion

This factor is characterised by contributions of 52%, 84% and 63% to the coal, peat and wood ATOFMS classes, respectively. The value for coal is lower than peat due to the input from power generation for the former. However, the contribution to the wood class is also relatively low when compared to peat, suggesting either another unidentified source or some incorrect distribution among the other factors. High contributions to the EC-domestic and oligomer particle classes are also observed (91% and 76%, respectively). This provides further support to indicate that oligomers are present in relatively fresh domestic combustion particles. This factor contributes 21% and 20% to the organic and elemental carbon measured, and is estimated to contribute 5% to the measured $PM_{2.5}$ mass.

3.3.6 Shipping

The shipping factor was not identified in the previous study of Hellebust et al. (2009), due to the absence of complementary ATOFMS data. A contribution of 100% is observed for the ATOFMS shipping class. This is expected, as these unique particles are emitted exclusively from container and liquid bulk vessels arriving and departing from the nearby shipping berths, with no input from other sources (Healy et al., 2009). Although shipping traffic is estimated to contribute only 1.5% to ambient $PM_{2.5}$ mass

ACPD
10, 1035–1082, 2010

during the sampling period, it contributes 18% to the total number of particles detected by the SMPS. This value is second only to traffic with a contribution of 42%. Thus it appears that local shipping traffic can contribute significantly to local ambient particle number in the size range 20–600 nm (mobility diameter) in Cork Harbour.

4 Conclusions

Over 550 000 ATOFMS particle mass spectra have been collected in Cork Harbour and clustered to generate 14 particle classes. The contribution of various local and regional sources to ambient levels of $PM_{2.5}$ mass in Cork Harbour has been estimated using positive matrix factorisation. The identified sources are estimated to account for 66% of the measured $PM_{2.5}$ mass. The combination of pre-clustered ATOFMS classes with PMF allows for a more refined identification of those sources. Furthermore, the distribution of the variable loadings of the ATOFMS classes among the six factors provide information that cannot be ascertained without the model, such as the separation of domestic and power generation-related coal burning and the identification of a marine organic carbon contribution. The identification of coal, peat and wood particle mass spectra in the ambient dataset was confirmed by burning these materials separately and measuring the resulting particles by ATOFMS. The uptake of nitrate by domestic combustion particles at night was observed to occur in the temporal order: wood, coal, peat, suggesting that hygroscopic growth factors for these particle classes decrease in the same order. Anthropogenic particles originating in North America or Canada were observed to contribute significantly to local $PM_{2.5}$ mass concentrations for the last 4 days of the measurement period. Approximately 33% of the measured $PM_{2.5}$ mass remains unaccounted for and possible missing sources include crustal material and biogenic secondary organic aerosol. A factor for crustal material was identified in a previous study focused on the off-line analysis of the metal content of $PM_{2.5}$ collected at a different site in Cork Harbour, and was estimated to contribute 11% to the measured $PM_{2.5}$ mass (Hellebust et al., 2009a). It is possible that crustal and biogenic

SOA particles were not detected by ATOFMS due to inefficient transmission through the aerodynamic lens or inefficient absorption of the UV laser. While local vehicular traffic was the largest source of ambient $PM_{2.5}$ mass in Cork Harbour during the sampling period, shipping traffic contributed significantly to ambient particle number. Considering that fresh ship exhaust particles reside predominantly in the ultrafine mode and contain polycyclic aromatic hydrocarbons and transition metals with known toxicological effects, this source may have implications for human health in the area (Fridell et al., 2008; Murphy et al., 2009; Healy et al., 2009; Sodeau et al., 2009).

Acknowledgements. The authors would like to acknowledge the Port of Cork for providing a suitable sampling site and Dave Cocker (University College Cork) for the use of the Agilent 5975 GC/MS instrument. This research has been funded by the Higher Education Authority, Ireland under PRTLI cycle IV, the Irish Environmental Protection Agency (STRIVE programme, 2006-EH-MS-49, 2007-PhD-EH6 and BIOCHEA) and Science Foundation Ireland (07/RFP/CHEF520).

References

Allan, J. D., Williams, P. I., Morgan, W. T., Martin, C. L., Flynn, M. J., Lee, J., Nemitz, E., Phillips, G. J., Gallagher, M. W., and Coe, H.: Contributions from transport, solid fuel burning and cooking to primary organic aerosols in two UK cities, Atmos. Chem. Phys. Discuss., 9, 19103–19157, 2009, http://www.atmos-chem-phys-discuss.net/9/19103/2009/.

Andreae, M. O. and Crutzen, P. J.: Atmospheric aerosols: biogeochemical sources and role in atmospheric chemistry, Science, 276, 1052–1058, doi:10.1126/science.276.5315.1052, 1997.

Ault, A. P., Moore, M. J., Furutani, H., and Prather, K. A.: Impact of emissions from the Los Angeles port region on San Diego air quality during regional transport events, Environ. Sci. Technol., 43, 3500–3506, doi:10.1021/es8018918, 2009.

Carlton, A. G., Turpin, B. J., Altieri, K. E., Seitzinger, S., Reff, A., Lim, H.-J., and Ervens, B.: Atmospheric oxalic acid and SOA production from glyoxal: results of aqueous photooxidation experiments, Atmos. Environ., 41, 7588–7602, 2007.

Carrico, C. M., Kreidenweis, S. M., Malm, W. C., Day, D. E., Lee, T., Carrillo, J., McMeeking, G. R., and Collett Jr, J. L.: Hygroscopic growth behavior of a carbon-dominated aerosol in Yosemite National Park, Atmos. Environ., 39, 1393–1404, 2005.

Castanho, A. D. A. and Artaxo, P.: Wintertime and summertime São Paulo aerosol source apportionment study, Atmos. Environ., 35, 4889–4902, 2001.

Dall'Osto, M., Beddows, D. C. S., Kinnersley, R. P., Harrison, R. M., Donovan, R. J., and Heal, M. R.: Characterization of individual airborne particles by using aerosol time-of-flight mass spectrometry at Mace Head, Ireland, J. Geophys. Res., 109, D21302, doi:21310.21029/22004JD004747, 2004.

Dall'Osto, M. and Harrison, R. M.: Chemical characterisation of single airborne particles in Athens (Greece) by ATOFMS, Atmos. Environ., 40, 7614–7631, 2006.

Denkenberger, K. A., Moffet, R. C., Holecek, J. C., Rebotier, T. P., and Prather, K. A.: Real-time, single-particle measurements of oligomers in aged ambient aerosol particles, Environ. Sci. Technol., 41, 5439–5446, doi:10.1021/es070329l, 2007.

Draxler, R. R. and Rolph, G. D.: HYSPLIT (Hybrid Single-Particle Lagrangian Integrated Trajectory) model v 4.9, NOAA Air Resource Laboratory, Silver Spring MD., http://www.arl.noaa.gov/ready/hysplit4.html, 2003.

Dreyfus, M. A., Adou, K., Zucker, S. M., and Johnston, M. V.: Organic aerosol source apportionment from highly time-resolved molecular composition measurements, Atmos. Environ., 43, 2901–2910, 2009.

Eatough, D. J., Grover, B. D., Woolwine, W. R., Eatough, N. L., Long, R., and Farber, R.: Source apportionment of 1 h semi-continuous data during the 2005 study of organic aerosols in riverside (SOAR) using positive matrix factorization, Atmos. Environ., 42, 2706–2719, 2008.

Forster, C., Wandinger, U., Wotawa, G., James, P., Mattis, I., Althausen, D., Simmonds, P., O'Doherty, S., Jennings, S. G., Kleefeld, C., Schneider, J., Trickl, T., Kreipl, S., Jager, H., and Stohl, A.: Transport of boreal forest fire emissions from Canada to Europe, J. Geophys. Res., 106, 22887–22906, 2001.

Fridell, E., Steen, E., and Peterson, K.: Primary particles in ship emissions, Atmos. Environ., 42, 1160–1168, 2008.

Friedman, B., Herich, H., Kammermann, L., Gross, D. S., Arneth, A., Holst, T., and Cziczo, D. J.: Subarctic atmospheric aerosol composition: 1. ambient aerosol characterization, J. Geophys. Res., 114, D13, doi:10.1029/2009jd011772, 2009.

Gard, E. E., Kleeman, M. J., Gross, D. S., Hughes, L. S., Allen, J. O., Morrical, B. D., Fer-

genson, D. P., Dienes, T., Galli, M. E., Johnson, R. J., Cass, G. R., and Prather, K. A.: Direct observation of heterogeneous chemistry in the atmosphere, Science, 279, 1184, doi:10.1126/science.279.5354.1184, 1998.

Godoy, M. L. D. P., Godoy, J. M., Roldão, L. A., Soluri, D. S., and Donagemma, R. A.: Coarse and fine aerosol source apportionment in Rio de Janeiro, Brazil, Atmos. Environ., 43, 2366–2374, 2009.

Gross, D. S., Galli, M. E., Silva, P. J., and Prather, K. A.: Relative sensitivity factors for alkali metal and ammonium cations in single-particle aerosol time-of-flight mass spectra, Anal. Chem., 72, 416–422, 2000.

Gross, D. S., Galli, M. E., Kalberer, M., Prevot, A. S. H., Dommen, J., Alfarra, M. R., Duplissy, J., Gaeggeler, K., Gascho, A., Metzger, A., and Baltensperger, U.: Real-time measurement of oligomeric species in secondary organic aerosol with the aerosol time-of-flight mass spectrometer, Anal. Chem., 78, 2130–2137, 2006a.

Gross, D. S., Schauer, J. J., Chen, L., Ramakrishnam, R., Ritz, A., and Musicant, D. R.: Enchilada: A Data-Mining Application for the Analysis of Atmospheric Mass Spectrometry Data, International Aerosol Conference, St. Paul, MN, USA, 2006b.

Guazzotti, S. A., Suess, D. T., Coffee, K. R., Quinn, P. K., Bates, T. S., Wisthaler, A., Hansel, A., Ball, W. P., Dickerson, R. R., Neusüß, C., Crutzen, P. J., and Prather, K. A.: Characterization of carbonaceous aerosols outflow from India and Arabia: Biomass/biofuel burning and fossil fuel combustion, J. Geophys. Res., 108, D15, doi:10.1029/2002jd003277, 2003.

Hallquist, M., Wenger, J. C., Baltensperger, U., Rudich, Y., Simpson, D., Claeys, M., Dommen, J., Donahue, N. M., George, C., Goldstein, A. H., Hamilton, J. F., Herrmann, H., Hoffmann, T., Iinuma, Y., Jang, M., Jenkin, M. E., Jimenez, J. L., Kiendler-Scharr, A., Maenhaut, W., McFiggans, G., Mentel, Th. F., Monod, A., Prévôt, A. S. H., Seinfeld, J. H., Surratt, J. D., Szmigielski, R., and Wildt, J.: The formation, properties and impact of secondary organic aerosol: current and emerging issues, Atmos. Chem. Phys., 9, 5155–5235, 2009, http://www.atmos-chem-phys.net/9/5155/2009/.

Healy, R. M., O'Connor, I. P., Hellebust, S., Allanic, A., Sodeau, J. R., and Wenger, J. C.: Characterisation of single particles from in-port ship emissions, Atmos. Environ., 43, 6408–6414, 2009.

Hellebust, S., Allanic, A., O'Connor, I. P., Jourdan, C., Healy, D., and Sodeau, J. R.: Sources of ambient concentrations and chemical composition of $PM_{2.5-0.1}$ in Cork Harbour, Ireland, Atmos. Res., doi:10.1016/j.atmosres.2009.09.006, in press, 2009a.

Hellebust, S., Allanic, A., O'Connor, I. P., Wenger, J. C., and Sodeau, J. R.: The use of real-time monitoring data to evaluate major sources of airborne particulate matter, Atmos. Environ., in press, 2009b.

Heo, J.-B., Hopke, P. K., and Yi, S.-M.: Source apportionment of $PM_{2.5}$ in Seoul, Korea, Atmos. Chem. Phys., 9, 4957–4971, 2009, http://www.atmos-chem-phys.net/9/4957/2009/.

Herich, H., Kammermann, L., Gysel, M., Weingartner, E., Baltensperger, U., Lohmann, U., and Cziczo, D. J.: In situ determination of atmospheric aerosol composition as a function of hygroscopic growth, J. Geophys. Res., 113, D162123, doi:10.1029/2008jd009954, 2008.

Herich, H., Kammermann, L., Friedman, B., Gross, D. S., Weingartner, E., Lohmann, U., Spichtinger, P., Gysel, M., Baltensperger, U., and Cziczo, D. J.: Subarctic atmospheric aerosol composition: 2. Hygroscopic growth properties, J. Geophys. Res., 114, D132204, doi:10.1029/2008jd011574, 2009.

Hopke, P. K.: Recent developments in receptor modeling, J. Chemometr., 17, 255–265, 2003a.

Hopke, P. K.: The evolution of chemometrics, Anal. Chim. Ac., 500, 365–377, 2003b.

Intergovernmental Panel on Climate Change (IPCC): Climate Change: The Scientific Basis, Cambridge University Press, UK, 2001.

Junninen, H., Mønster, J., Rey, M., Cancelinha, J., Douglas, K., Duane, M., Forcina, V., Müller, A., Lagler, F., Marelli, L., Borowiak, A., Niedzialek, J., Paradiz, B., Mira-Salama, D., Jimenez, J., Hansen, U., Astorga, C., Stanczyk, K., Viana, M., Querol, X., Duvall, R. M., Norris, G. A., Tsakovski, S., Wåhlin, P., Horaìk, J., and Larsen, B. R.: Quantifying the impact of residential heating on the urban air quality in a typical european coal combustion region, Environ. Sci. Technol., 43, 7964–7970, doi:10.1021/es8032082, 2009.

Kalberer, M., Paulsen, D., Sax, M., Steinbacher, M., Dommen, J., Prevot, A. S. H., Fisseha, R., Weingartner, E., Frankevich, V., Zenobi, R., and Baltensperger, U.: Identification of polymers as major components of atmospheric organic aerosols, Science, 303, 1659–1662, 2004.

Karanasiou, A. A., Siskos, P. A., and Eleftheriadis, K.: Assessment of source apportionment by positive matrix factorization analysis on fine and coarse urban aerosol size fractions, Atmos. Environ., 43, 3385–3395, 2009.

Kourtchev, I., Warnke, J., Maenhaut, W., Hoffmann, T., and Claeys, M.: Polar organic marker compounds in $PM_{2.5}$ aerosol from a mixed forest site in Western Germany, Chemosphere, 73, 1308–1314, 2008.

Kourtchev, I., Bejan, I., Sodeau, J. R., and Wenger, J. C.: Gas-phase reaction of (E)-[beta]-

farnesene with ozone: rate coefficient and carbonyl products, Atmos. Environ., 43, 3182–3190, 2009a.

Kourtchev, I., Bell, J., Hellebust, S., O'Connor, I., Allanic, A., Healy, R. M., Healy, D., Wenger, J. C., and Sodeau, J. R.: Organic composition of $PM_{2.5}$ aerosols in Cork Harbour, Ireland, European Aerosol Conference, Karlsruhe, Germany 2009b.

Kundu, S., Kawamura, K., Andreae, T. W., Hoffer, A., and Andreae, M. O.: Molecular distributions of dicarboxylic acids, ketocarboxylic acids and α-dicarbonyls in biomass burning aerosols: implications for photochemical production and degradation in smoke layers, Atmos. Chem. Phys. Discuss., 9, 19783–19815, 2009, http://www.atmos-chem-phys-discuss.net/9/19783/2009/.

Lanz, V. A., Alfarra, M. R., Baltensperger, U., Buchmann, B., Hueglin, C., and Prévôt, A. S. H.: Source apportionment of submicron organic aerosols at an urban site by factor analytical modelling of aerosol mass spectra, Atmos. Chem. Phys., 7, 1503–1522, 2007, http://www.atmos-chem-phys.net/7/1503/2007/.

MacQueen, J.: Some methods for classification and analysis of multivariate observations, Fifth Berkeley Symposium on Mathematical Statistics and Probability, 1967.

Maier, K. L., Alessandrini, F., Beck-Speier, I., Hofer, T. P. J., Diabate, S., Bitterle, E., Stoger, T., Jakob, T., Behrendt, H., Horsch, M., Beckers, J., Ziesenis, A., Hultner, L., and Frankenberger, M.: Health effects of ambient particulate matter – biological mechanisms and inflammatory responses to in vitro and in vivo particle exposures, Inhal. Toxicol., 20, 319–337, 2008.

Maykut, N. N., Lewtas, J., Kim, E., and Larson, T. V.: Source apportionment of $PM_{2.5}$ at an urban IMPROVE site in Seattle, Washington, Environ. Sci. Technol., 37, 5135–5142, doi:10.1021/es030370y, 2003.

Mira-Salama, D., Grüning, C., Jensen, N. R., Cavalli, P., Putaud, J. P., Larsen, B. R., Raes, F., and Coe, H.: Source attribution of urban smog episodes caused by coal combustion, Atmos. Res., 88, 294–304, 2008.

Moffet, R. C., de Foy, B., Molina, L. T., Molina, M. J., and Prather, A.: Measurement of ambient aerosols in northern Mexico City by single particle mass spectrometry, Atmos. Chem. Phys., 8, 4499–4516, 2008, http://www.atmos-chem-phys.net/8/4499/2008/.

Mogili, P. K., Kleiber, P. D., Young, M. A., and Grassian, V. H.: N_2O_5 hydrolysis on the components of mineral dust and sea salt aerosol: comparison study in an environmental aerosol

reaction chamber, Atmos. Environ., 40, 7401–7408, 2006.
Mugica, V., Ortiz, E., Molina, L., De Vizcaya-Ruiz, A., Nebot, A., Quintana, R., Aguilar, J., and Alcántara, E.: PM composition and source reconciliation in Mexico City, Atmos. Environ., 43, 5068–5074, 2009.
Murphy, S. M., Agrawal, H., Sorooshian, A., Padro, L. T., Gates, H., Hersey, S., Welch, W. A., Jung, H., Miller, J. W., Cocker, D. R., Nenes, A., Jonsson, H. H., Flagan, R. C., and Seinfeld, J. H.: Comprehensive simultaneous shipboard and airborne characterization of exhaust from a modern container ship at sea, Environ. Sci. Technol., 43, 4626–4640, doi:10.1021/es802413j, 2009.
Paatero, P. and Tapper, U.: Positive matrix factorisation – a nonnegative factor model with optmal utilisation of error-estimates of data values, Environmetrics, 5, 111–126, 1994.
Pashynska, V., Vermeylen, R., Vas, G., Maenhaut, W., and Claeys, M.: Development of a gas chromatographic/ion trap mass spectrometric method for the determination of levoglucosan and saccharidic compounds in atmospheric aerosols. Application to urban aerosols, J. Mass Spectrom., 37, 1249–1257, 2002.
Ramadan, Z., Eickhout, B., Song, X.-H., Buydens, L. M. C., and Hopke, P. K.: Comparision of positive matrix factorisation and multilinear engine for the source apportionment of particulate pollutants, Chemometr. Intell. Lab., 66, 15–28, 2003.
Reinard, M. S., Adou, K., Martini, J. M., and Johnston, M. V.: Source characterization and identification by real-time single particle mass spectrometry, Atmos. Environ., 41, 9397–9409, 2007.
Rissler, J., Vestin, A., Swietlicki, E., Fisch, G., Zhou, J., Artaxo, P., and Andreae, M. O.: Size distribution and hygroscopic properties of aerosol particles from dry-season biomass burning in Amazonia, Atmos. Chem. Phys., 6, 471–491, 2006, http://www.atmos-chem-phys.net/6/471/2006/.
Shi, G.-L., Li, X., Feng, Y.-C., Wang, Y.-Q., Wu, J.-H., Li, J., and Zhu, T.: Combined source apportionment, using positive matrix factorization-chemical mass balance and principal component analysis/multiple linear regression-chemical mass balance models, Atmos. Environ., 43, 2929–2937, 2009.
Silva, P. J., Liu, D. Y., Noble, C. A., and Prather, K. A.: Size and chemical characterization of individual particles resulting from biomass burning of local Southern California species, Environ. Sci. Technol., 33, 3068–3076, 1999.
Silva, P. J. and Prather, K. A.: Interpretation of mass spectra from organic compounds in aerosol

time-of-flight mass spectrometry, Anal. Chem., 72, 3553–3562, 2000.
Simoneit, B. R. T., Elias, V. O., Kobayashi, M., Kawamura, K., Rushdi, A. I., Medeiros, P. M., Rogge, W. F., and Didyk, B. M.: Sugars-dominant water-soluble organic compounds in soils and characterization as tracers in atmospheric particulate matter, Environ. Sci. Technol., 38, 5939–5949, doi:10.1021/es0403099, 2004.
Snyder, D. C., Schauer, J. J., Gross, D. S., and Turner, J. R.: Estimating the contribution of point sources to atmospheric metals using single-particle mass spectrometry, Atmos. Environ., 43, 4033–4042, 2009.
Sodeau, J., Hellebust, S., Allanic, A., O'Connor, I., Healy, D., Healy, R., and Wenger, J.: Airborne emissions in the harbour and port of Cork, Biomarkers, 14, 12–16, 2009.
Spencer, M. T., Shields, L. G., Sodeman, D. A., Toner, S. M., and Prather, K. A.: Comparison of oil and fuel particle chemical signatures with particle emissions from heavy and light duty vehicles, Atmos. Environ., 40, 5224–5235, 2006.
Stohl, A., Forster, C., Eckhardt, S., Spichtinger, N., Huntrieser, H., Heland, J., Schlager, H., Wilhelm, S., Arnold, F., and Cooper, O.: A backward modeling study of intercontinental pollution transport using aircraft measurements, J. Geophys. Res., 108, 4370, doi:10.1029/2002JD002862, 2003.
Sullivan, R. C. and Prather, K. A.: Recent advances in our understanding of atmospheric chemistry and climate made possible by on-line aerosol analysis instrumentation, Anal. Chem., 77, 3861–3885, 2005.
Sullivan, R. C., Guazzotti, S. A., Sodeman, D. A., and Prather, K. A.: Direct observation of the atmospheric processing of Asian mineral dust, Atmos. Chem. Phys., 7, 1213–1236, 2007, http://www.atmos-chem-phys.net/7/1213/2007/.
Sullivan, R. C. and Prather, K. A.: Investigations of the diurnal cycle and mixing state of oxalic acid in individual particles in Asian aerosol outflow, Environ. Sci. Technol., 41, 8062–8069, 2007.
Toner, S. M., Sodeman, D. A., and Prather, K. A.: Single particle characterization of ultrafine and accumulation mode particles from heavy duty diesel vehicles using aerosol time-of-flight mass spectrometry, Environ. Sci. Technol., 40, 3912–3921, 2006.
Toner, S. M., Shields, L. G., Sodeman, D. A., and Prather, K. A.: Using mass spectral source signatures to apportion exhaust particles from gasoline and diesel powered vehicles in a freeway study using UF-ATOFMS, Atmos. Environ., 42, 568–581, 2008.
Ulbrich, I. M., Canagaratna, M. R., Zhang, Q., Worsnop, D. R., and Jimenez, J. L.: Interpreta-

tion of organic components from Positive Matrix Factorization of aerosol mass spectrometric data, Atmos. Chem. Phys., 9, 2891–2918, 2009, http://www.atmos-chem-phys.net/9/2891/2009/.

Wang, X., Zhang, Y., Chen, H., Yang, X., Chen, J., and Geng, F.: Particulate Nitrate Formation in a highly polluted urban area: a case study by single-particle mass spectrometry in Shanghai, Environ. Sci. Technol., 43, 3061–3066, doi:10.1021/es8020155, 2009.

Weingartner, E., Burtscher, H., and Baltensperger, U.: Hygroscopic properties of carbon and diesel soot particles, Atmos. Environ., 31, 2311–2327, 1997.

Yang, F., Chen, H., Wang, X., Yang, X., Du, J., and Chen, J.: Single particle mass spectrometry of oxalic acid in ambient aerosols in Shanghai: mixing state and formation mechanism, Atmos. Environ., 43, 3876–3882, 2009.

Yin, J., Allen, A. G., Harrison, R. M., Jennings, S. G., Wright, E., Fitzpatrick, M., Healy, T., Barry, E., Ceburnis, D., and McCusker, D.: Major component composition of urban PM_{10} and $PM_{2.5}$ in Ireland, Atmos. Res., 78, 149–165, 2005.

Zhang, Y., Schauer, J. J., Zhang, Y., Zeng, L., Wei, Y., Liu, Y., and Shao, M.: Characteristics of particulate carbon emissions from real-world Chinese coal combustion, Environ. Sci. Technol., 42, 5068–5073, 2008.

Table 1. Mean, median, maximum and minimum hourly average mass concentrations for semi-continuous measurements at the Tivoli Docks from 7–28 August 2008 ($\mu g\,m^{-3}$).

	OC	EC	SO_4^{2-}	$PM_{2.5}$
Mean	1.13	0.61	0.49	9.67
Median	1.02	0.55	0.45	8.55
Maximum	3.41	2.90	2.14	49.80
Minimum	0.22	0.00	0.04	1.50

Table 2. Correlation coefficient squared (R^2) values for the least squares linear regression of coal, peat and wood particle counts and galactosan, mannosan and levoglucosan mass concentrations (n=17).

	Coal	Peat	Wood	Galactosan	Mannosan	Levoglucosan
Coal	1	0.91	0.92	0.68	0.57	0.82
Peat	0.91	1	0.9	0.59	0.53	0.82
Wood	0.92	0.9	1	0.56	0.46	0.81
Galactosan	0.68	0.59	0.56	1	0.9	0.79
Mannosan	0.57	0.53	0.46	0.9	1	0.75
Levoglucosan	0.82	0.82	0.81	0.79	0.75	1

Table 3. Percentage variable contributions to the six factor PMF model and estimated percentage contribution of each factor to the measured ambient $PM_{2.5}$ mass.

	Traffic	Marine	Long-range	Power generation	Domestic combustion	Shipping
Quantitative measurements						
OC mass	20.65	19.93	18.05	16.16	20.90	4.31
EC mass	43.27	4.58	10.73	18.35	19.52	3.55
Sulfate mass	8.84	23.41	15.28	39.84	10.50	2.14
Particle number*	41.81	6.42	6.77	13.08	14.00	17.91
ATOFMS classes						
Coal	4.78	2.87	7.32	29.84	51.73	3.45
Peat	3.29	2.33	3.17	4.96	84.26	1.98
Wood	11.39	13.17	6.09	5.28	62.96	1.10
Sea salt	1.32	86.14	9.70	1.72	0.15	0.97
Shipping	0	0	0	0	0	100
Ca-traffic	82.76	4.42	8.47	0	0	4.35
EC-traffic	58.84	0.91	2.74	6.07	25.46	5.97
EC-phos-fresh	81.85	0.00	6.10	2.64	9.21	0.20
EC-phos-aged	0.83	5.92	89.89	3.04	0.31	0
EC-domestic	0	0	1.97	0.00	90.56	7.47
EC-background	27.57	1.35	11.45	35.38	17.79	6.47
EC-oil	51.98	0.64	0	23.70	23.67	0
OC	0	0.00	30.57	69.06	0	0.37
Oligomer	0.17	14.71	0	8.01	76.19	0.91
$PM_{2.5}$	22.92	13.68	12.68	10.68	4.87	1.49

* Mobility diameter range 20–600 nm.

ACPD
10, 1035–1082, 2010

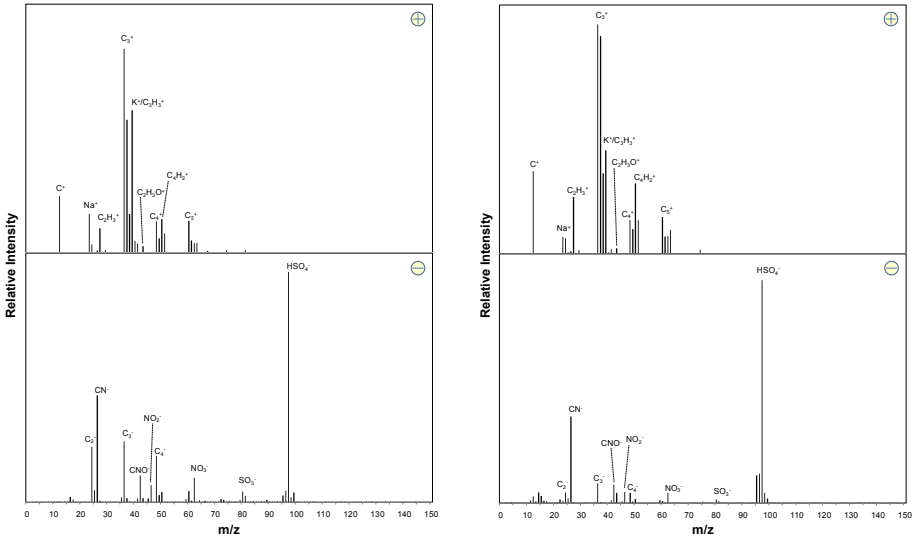

Fig. 1. Average dual ion mass spectra of ambient particles classified as coal-fresh (left) and particles sampled during the coal combustion experiment (right).

ACPD
10, 1035–1082, 2010

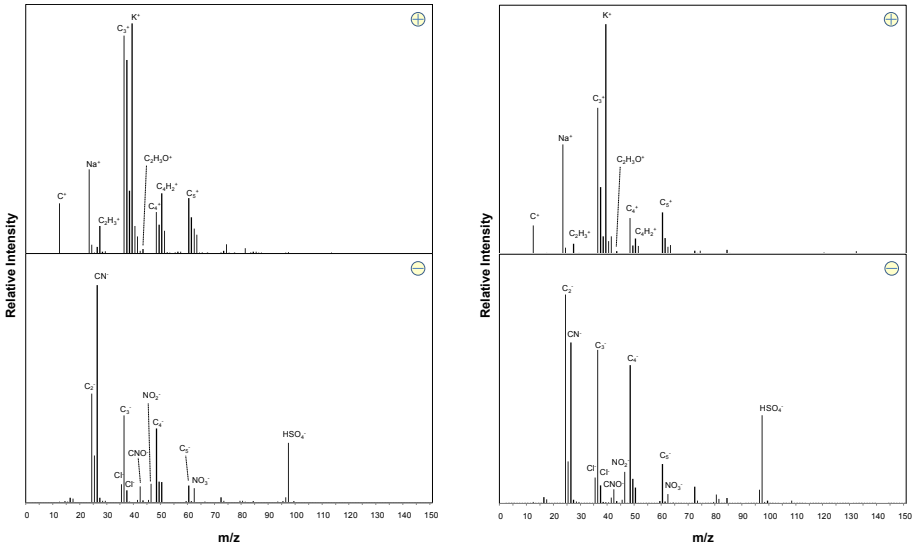

Fig. 2. Average dual ion mass spectra of ambient particles classified as peat-fresh (left) and particles sampled during the peat combustion experiment (right).

ACPD
10, 1035–1082, 2010

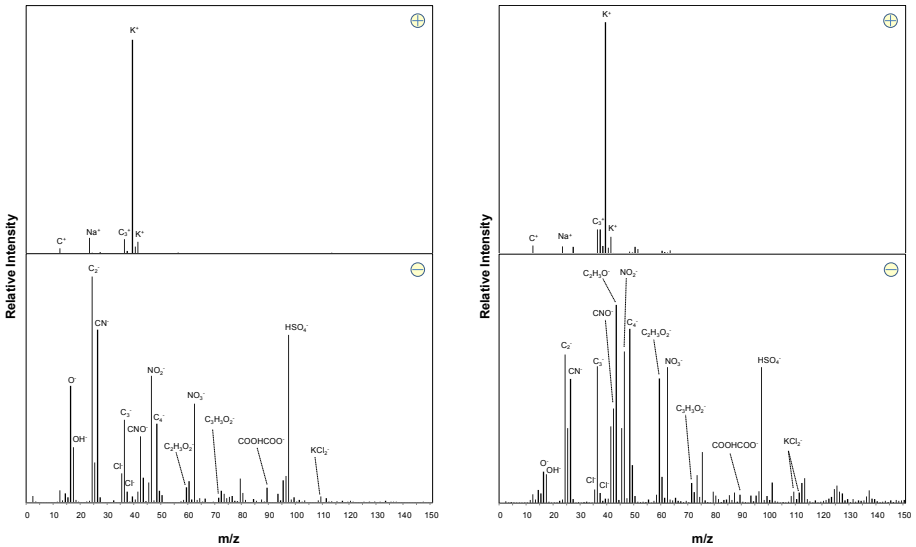

Fig. 3. Average dual ion mass spectra of ambient particles classified as wood-fresh (left) and particles sampled during the wood combustion experiment (right).

ACPD
10, 1035–1082, 2010

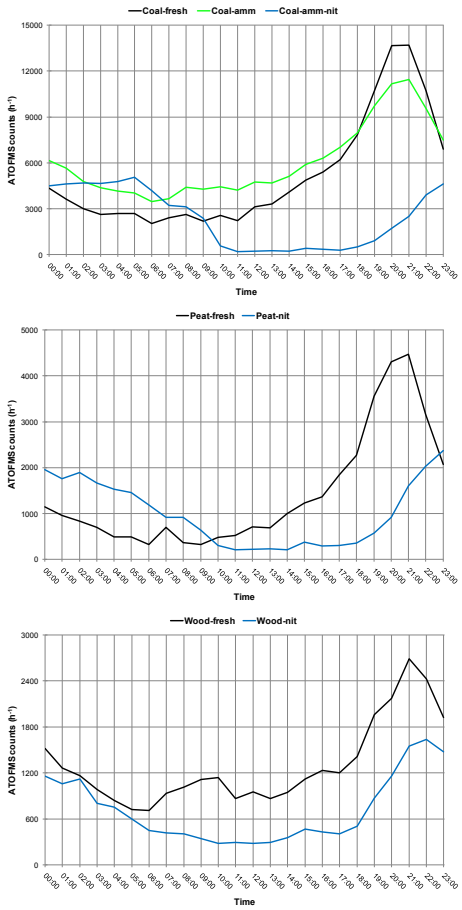

Fig. 4. Average diurnal trends for coal (top), peat (middle), and wood (bottom) subclass particle counts. Coal-fresh particle number has been multiplied by a factor of 5 for clarity.

ACPD
10, 1035–1082, 2010

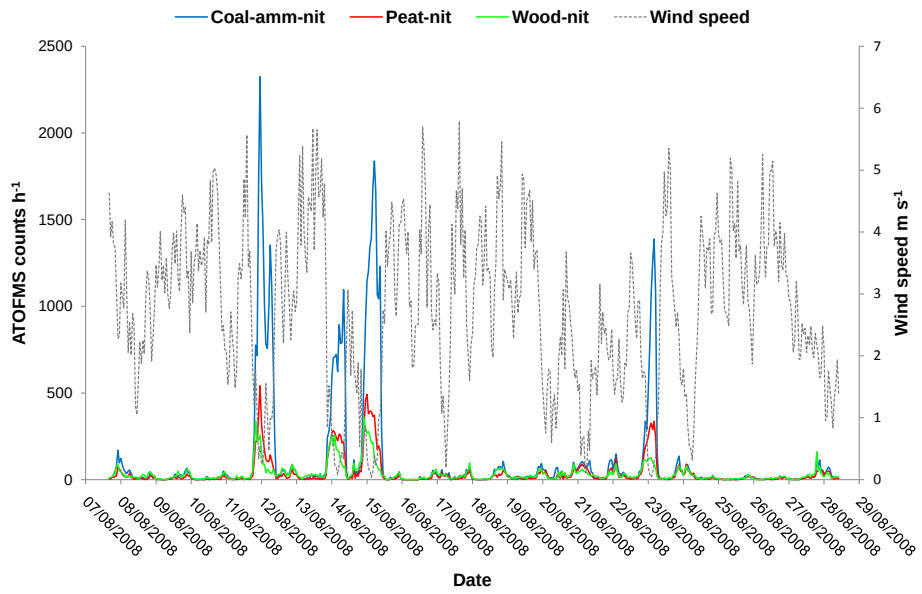

Fig. 5. Hourly summed particle counts for the coal-amm-nit, peat-nit and wood-nit subclasses and hourly averaged wind speed values for 7–28 August 2008.

ACPD
10, 1035–1082, 2010

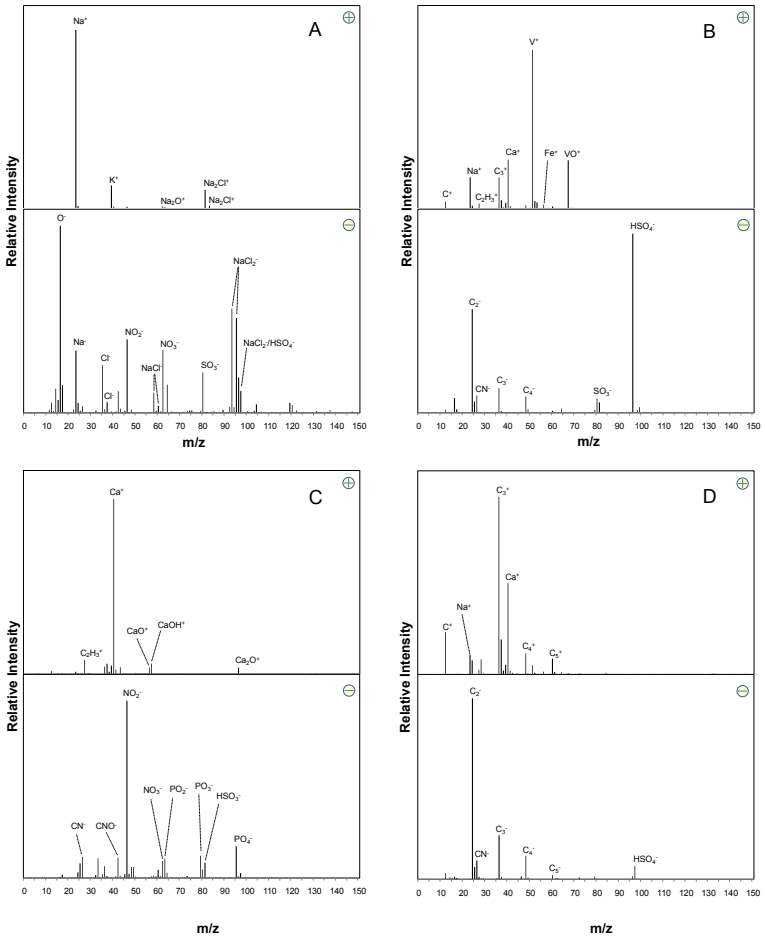

Fig. 6. Average dual ion mass spectra of ATOFMS particle classes; **(A)** sea salt, **(B)** shipping, **(C)** Ca-traffic, **(D)** EC-traffic.

ACPD
10, 1035–1082, 2010

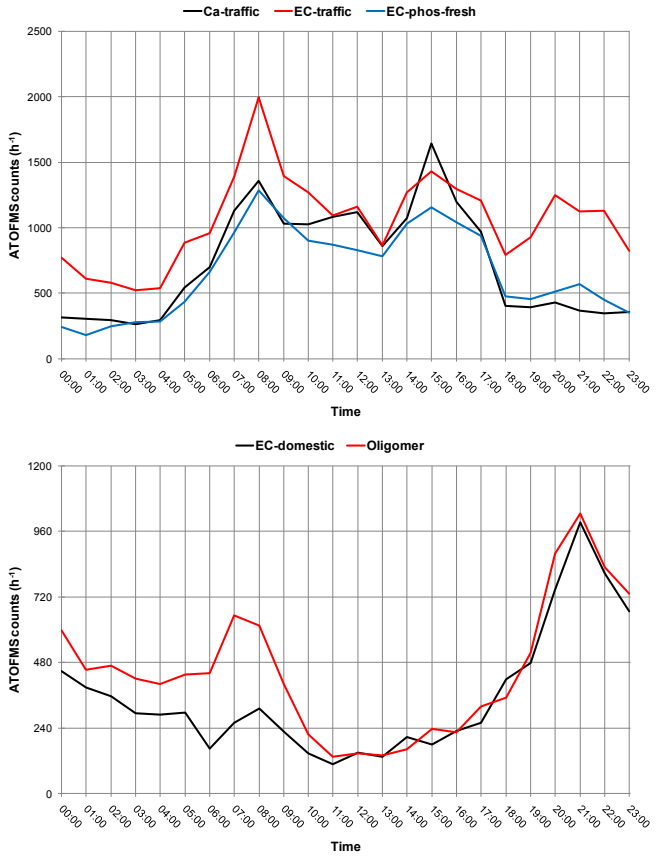

Fig. 7. Average diurnal trend for (top) Ca-traffic, EC-traffic and EC-phos-fresh and (bottom) EC-domestic and oligomer particle counts. EC-phos-fresh and EC-domestic particle numbers have been multiplied by a factor of 3 and 1.5, respectively for comparative purposes.

ACPD
10, 1035–1082, 2010

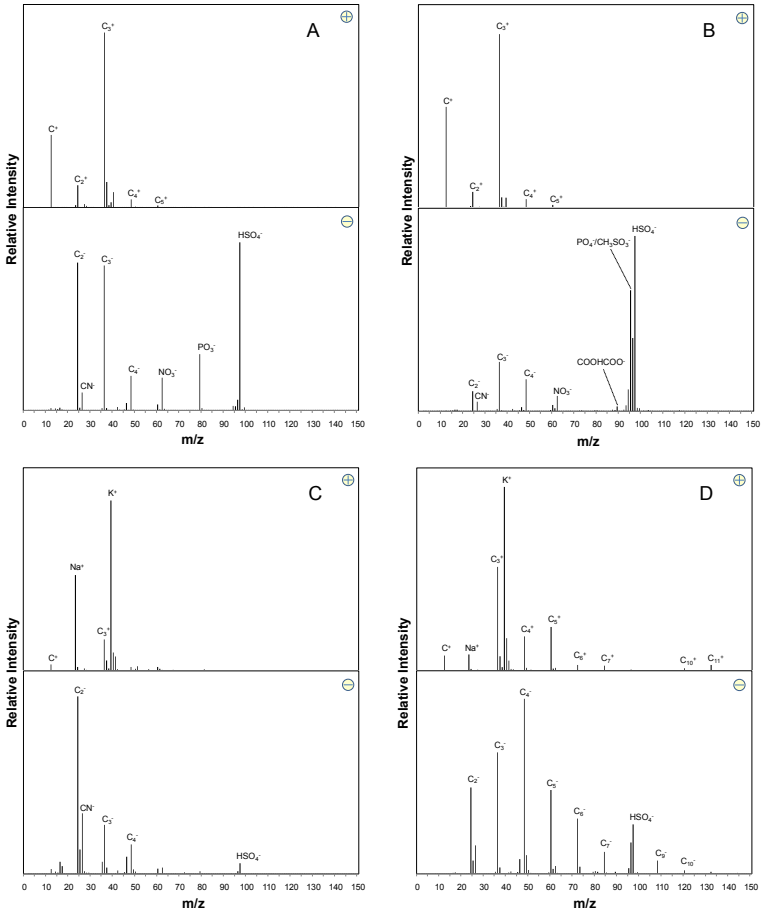

Fig. 8. Average dual ion mass spectra of ATOFMS particle classes; **(A)** EC-phos-fresh, **(B)** EC-phos-aged, **(C)** EC-domestic **(D)** EC-background.

ACPD
10, 1035–1082, 2010

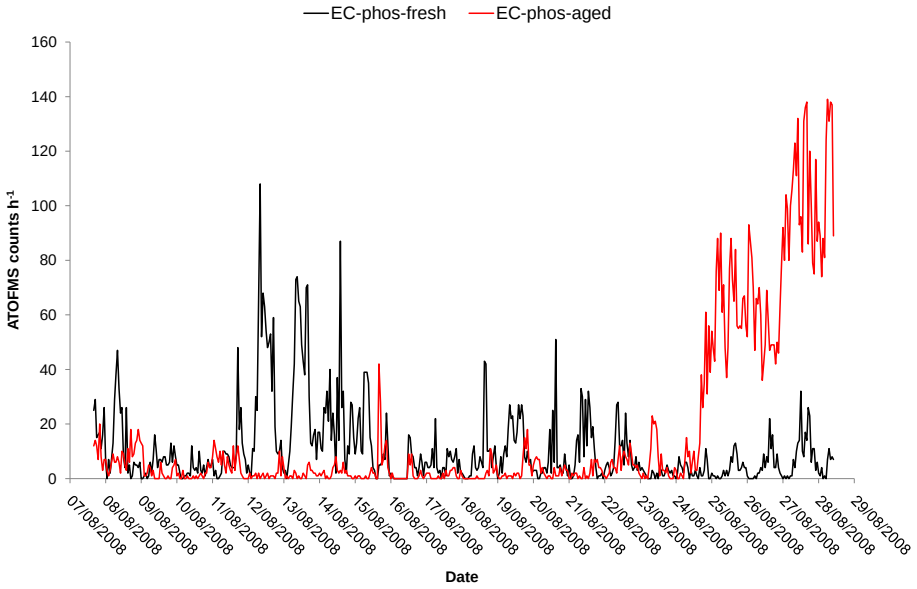

Fig. 9. Hourly summed particle counts for EC-phos-fresh and EC-phos-aged particles for 7–28 August 2008.

ACPD
10, 1035–1082, 2010

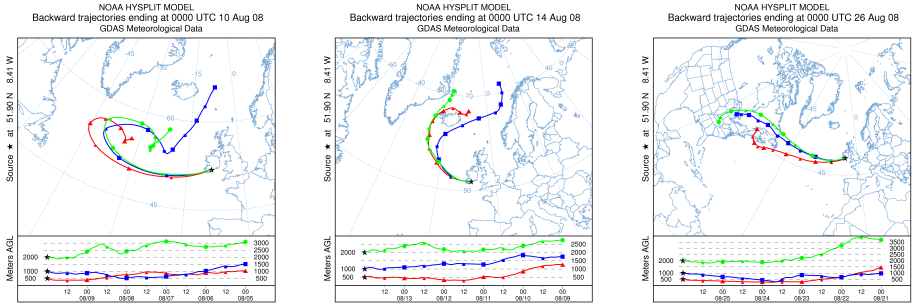

Fig. 10. 5 day back-trajectories for air masses arriving at Cork Harbour on at 00:00 h on 10 (left), 14 (middle) and 26 August 2008 (right).

ACPD
10, 1035–1082, 2010

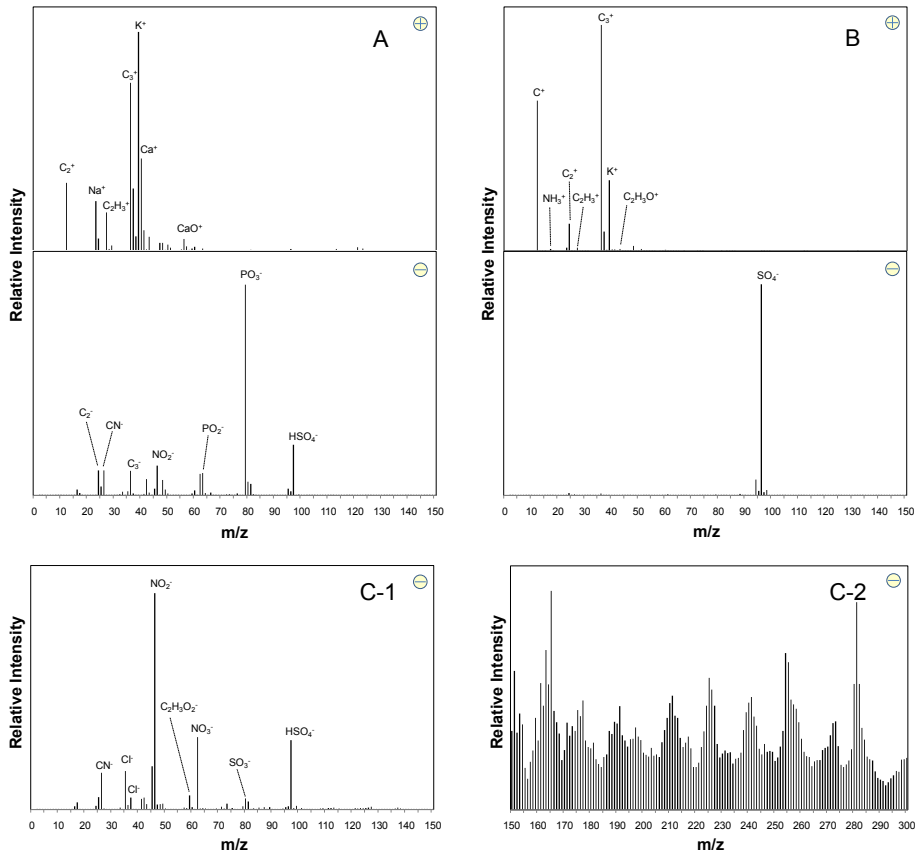

Fig. 11. Average dual ion mass spectra of ATOFMS particle classes; **(A)** EC-oil, **(B)** OC, and average negative ion mass spectra for **(C-1)** oligomer (*m/z* 0–150) and **(C-2)** oligomer (*m/z* 150–300).

ACPD
10, 1035–1082, 2010